Electronic Supplementary Material (ESI) for Energy & Environmental Science.

Supporting Information

Closely packed $Pt_{1.5}Ni_{1-x}$/Ni-N-C hybrid for relay catalysis towards oxygen reduction

Wenxin Guo,[†ab] *Xiaoping Gao,*[†a] *Mengzhao Zhu,*[†a] *Chenxi Xu,*[c] *Xiaorong Zhu,*[d] *Xuyan Zhao,*[a] *Rongbo Sun,*[a] *Zhenggang Xue,*[e] *Jia Song,*[a] *Lin Tian,*[a] *Jie Xu,*[f] *Wenxing Chen,*[g] *Yue Lin,*[h] *Yafei Li,*[i] *Huang Zhou**[a] *and Yuen Wu**[ab]

[a] Department of Chemistry, iChEM (Collaborative Innovation Center of Chemistry for Energy Materials), University of Science and Technology of China, Hefei 230026, China.

[b] Dalian National Laboratory for Clean Energy, Dalian 116023, China

[c] School of Materials Science and Engineering, Hefei University of Technology, Hefei 230009, China

[d] School of Chemistry and Chemical Engineering, Nantong University, Nantong 226019, China

[e] NEST Laboratory, Department of Physics, Department of Chemistry, College of Science, Shanghai University, Shanghai 200444, China

[f] Institute of Functional Nano and Soft Materials (FUNSOM), Jiangsu Key Laboratory for Carbon-Based Functional Materials & Devices, Soochow University, Suzhou 215123, China

[g] Beijing Key Laboratory of Construction Tailorable Advanced Functional Materials and Green Applications, School of Materials Science and Engineering, Beijing Institute of Technology, Beijing 100081, China

[h] Hefei National Research Center for Physical Sciences at the Microscale , University of Science and Technology of China, Hefei 230026, China

[i] Jiangsu Collaborative Innovation Centre of Biomedical Functional Materials, School of Chemistry and Materials Science, Nanjing Normal University, Nanjing 210023, China

† These authors contributed equally.

1.EXPERIMENTAL SECTION

Chemicals

All chemicals were used as received without further purification. Platinum (II) 2,4-pentanedionate ($Pt(acac)_2$, Pt 48.0%), Nickel acetylacetonate ($Ni(acac)_2$) and commercial Pt/C was purchased from Alfa Aesar. Zinc nitrate hexahydrate ($Zn(NO_3)_2 \cdot 6H_2O$) and 2-methylimidazole were obtained from Shanghai Chemical Reagent. N, N-Dimethylformamide (DMF), methanol (MeOH) and alcohol (EtOH) was purchased from Sinopharm Chemical Reagent Co., Ltd (Shanghai, China). Deionized (DI) water from Milli-Q System (Millipore, Billerica, MA) was used in all our experiments. 5 wt % Nafion solution was purchased from Aldrich. The commercial Pt/C catalyst is 20 wt % of ~3 nm Pt nanoparticles on Vulcan XC-72 carbon support.

Materials synthesis

Synthesis of ZIF-8

Typically, 0.558 g $Zn(NO_3)_2 \cdot 6H_2O$ was dissolved in 20 mL methanol and subsequently added to 20 mL methanol containing 0.616 g 2-methylimidazole under ultrasound for 10 minutes at room temperature. The ZIF-8 was then grown under static at 25°C for 12 hours. As-obtained precipitates were centrifuged, washed three times with methanol and dried in vacuum at 65°C overnight.

Synthesis of N-doped C

The powder of ZIF-8 was placed in a tube furnace, kept at 900°C for 1 hour and 1000°C for 1 hour successively with a heating rate of 5°C min^{-1} under flowing argon gas, and then naturally cooled to room temperature. As-prepared samples were then immersed in 0.5M H_2SO_4 and stirred at room temperature for 12h to completely remove the residual Zn species.

Synthesis of $Pt_{1.5}Ni$/N-C

The $Pt_{1.5}Ni$ octahedral nanoparticles were synthesized by completely dissolving 4 mM $Pt(acac)_2$ and 3 mM $Ni(acac)_2$ into 100 mL pure DMF. Then, the precursor solutions were transferred into a Teflon-lined stainless-steel autoclave. The mixed solutions in sealed autoclave were heated from room temperature to 120°C within 10 minutes and the heating rate is ~10°C/min, $Pt_{1.5}Ni$ octahedral nanoparticles were synthesized after reaction of 42 hours. Before washing the particles, the N-doped C was added to the mixing solution. Finally, $Pt_{1.5}Ni$/N-C was obtained by washing with ethanol several times and followed by drying in a vacuum oven at 60°C.

Synthesis of $Pt_{1.5}Ni_{1-x}$/Ni-N-C

Typically, the powder of $Pt_{1.5}Ni$/N-C was placed in a tube furnace, kept at 300°C for 4 hours with a heating rate of 5°C min^{-1} under flowing NH_3 gas, and then naturally cooled to room temperature. The obtained product was denoted as $Pt_{1.5}Ni_{1-x}$/Ni-N-C. The sample of $Pt_{1.5}Ni$/N-C kept at 150°C and 250°C for 4 hours with same heating conditions above were denoted as treated at 150°C and treated at 250°C, respectively. As-prepared samples were directly used without any post-treatment.

Synthesis of Ni SAs/N-C.

As-prepared N-doped C derived from ZIF-8 powder (100 mg) was dispersed in hexane (10 ml) and sonicated for 5 min at room temperature. After forming a homogeneous solution, an aqueous $Ni(NO_3)_2$ solution (100 mg ml^{-1}, 50μL) was slowly injected by sonication at room temperature for 2min. The mixed solution was then stirred vigorously at room temperature for 3h to allow complete absorption of the salt solution. Then the samples were centrifuged and dried under vacuum at 65 °C for 6 h. The samples were placed in a tube furnace and heated to 1000 °C (heating rate 5°C/min) in a stream of argon (10 ml/min) for 2 h to produce Ni SAs/N-C.

Materials characterizations

Characterization XRD measurements were recorded on a Rigaku Miniflex-600 operated at 40 kV voltage and 15 mA current using a Cu Kα radiation (λ=0.15406 nm) at a step width of 2° min^{-1}. TEM images were recorded on a Hitachi-7700 worked at 100 kV. The high-resolution TEM (HRTEM) and the corresponding EDS were recorded on JEOL JEM-2100F field-emission electron microscope at 200 kV. HAADF-STEM images were recorded on a FEI Titan Cubed Themis G2 300 with a probe corrector at 200 kV. X-ray photoelectron spectroscopy (XPS, VG-Multilab2000) was performed by using Al Kα radiation (1486.71 eV). Elemental analysis of Pt and Ni in the solid samples was detected by inductively coupled plasma atomic emission spectrometry (Optima 7300 DV). Raman shifts were carried out by using a LabRAM

Aramis Raman spectrometer instrument with an excitation wavelength of 514 nm using the Ar ion laser. The BET (Brunauer-Emmett-Teller) test was obtained from micromeritics ASAP 2020 HD88 PLUS. All the samples were degassed at 573 K for 3 h. Soft X-ray absorption spectra (Soft-XAS, C K-edge and N-Kedge) were carried out at BL12B X-ray Magnetic Circular Dichroism (XMCD) station and BL10B photoemission end-station of National Synchrotron Radiation Laboratory (NSRL, Hefei in China) in TEY mode. The X-ray absorption fine structure data (Ni K-edge) was collected at 1W1B station in Beijing Synchrotron Radiation Facility (BSRF). The storage rings of BSRF were operated at 2.5 GeV with a maximum current of 250 mA. The data was collected at room temperature in transmission mode using N_2-filled ionization chamber. All samples were pelletized as disks of 13 mm diameter using graphite powder as a binder. The acquired EXAFS data was processed according to the standard procedures using the ATHENA module implemented in the IFEFFIT software packages. The EXAFS spectra were obtained by subtracting the post-edge background from the overall absorption and then normalizing with respect to the edge-jump step. Subsequently, $\chi(k)$ data in the k-space was Fourier transformed to real (R) space using a hanning windows (dk=1.0 Å^{-1}) to separate the EXAFS contributions from different coordination shells.

Electrochemical measurements for ORR

All electrochemical experiments were conducted on a CHI 760E electrochemical workstation (Shanghai Chenhua, China) in a conventional three-electrode system at room temperature. Samples were tested using the glassy carbon electrode (GCE, 5 mm diameter, 0.196 cm^2) as the working electrode, Ag/AgCl as the reference electrode and a graphite rod as the counter electrode. The catalyst solutions were prepared by mixing 4 mg of catalysts in a solution containing 490 μL of ethanol, 490 μL of H_2O and 20 μL of 5% Nafion solution by sonication for 1 hour to form homogeneous catalyst inks. While, commercial 20% Pt/C sample was prepared by dispersing 4 mg of the catalyst in 1 mL of solution. Next, a certain volume of the catalyst ink was carefully dropped onto the polished glassy carbon rotating disk electrode (RDE) or rotating ring disk electrode (RRDE), leading to a desirable catalyst loading. The Pt loadings were 0.008 mg cm^{-2}, 0.008mg cm^{-2} and 0.0150 mg cm^{-2} for $Pt_{1.5}Ni_{1-x}$/Ni-N-C,

$Pt_{1.5}Ni/N\text{-}C$ and commercial Pt/C respectively. (All the loading mass were normalized over the geometric electrode area of 0.196 cm^2). Cyclic voltammetry (CV) activations were performed in N_2/O_2-saturated 0.1 M $HClO_4$ electrolyte with potential scan rate of 10 mV s^{-1}. All the electrochemical active surface area (ECSA) was determined by integrating hydrogen adsorption charge on CV curve by assuming a value of 210 μC cm^{-2} for the adsorption of a hydrogen monolayer. Double-layer correction was applied. The ECSA for $Pt_{1.5}Ni_{1-x}/Ni\text{-}N\text{-}C$, $Pt_{1.5}Ni$ N-C and Pt/C were calculated via same method. Oxygen reduction reaction (ORR) tests were conducted in O_2-saturated 0.1 M $HClO_4$ electrolyte with potential scan rate of 10 mV s^{-1}. The RDE tests were measured at rotating speed of 1600 rpm with a sweep rate of 10 mV s^{-1}.

$$\frac{1}{J}=\frac{1}{J_L}+\frac{1}{J_K}=\frac{1}{B\omega^{1/2}}+\frac{1}{J_K} \qquad (1)$$

$$B=0.62nFC_0{D_0}^{2/3}v^{-1/6} \qquad (2)$$

where J is the measured current density, J_K and J_L are the kinetic and diffusion-limiting current densities, ω is the angular velocity, n is transferred electron number, F is the Faraday constant (96, 485 C mol^{-1}), C_0 is the bulk concentration of O_2 (1.26×10^{-6} mol cm^{-3}), D_0 is the diffusion coefficient of O_2 (1.90×10^{-5} cm^2 s^{-1}), and V is the kinematic viscosity of the electrolyte (0.01 cm^2 s^{-1}).

The specific kinetic current density can be calculated from K-L equation:

$$J_K=\frac{J_L * J}{J_L-J} \qquad (3)$$

For RRDE tests, a computer-controlled CHI 760E electrochemical workstation was employed and the disk electrode was scanned catholically at a rate of 20 mV s^{-1} and the ring electrode potential was set to 1.20 V vs. RHE. The hydrogen peroxide yield (H_2O_2%) and the electron transfer number (n) were determined by the following equations:

$$H_2O_2(\%)=200\frac{i_r/N}{i_d+i_r/N} \qquad (4)$$

$$n=4\frac{i_d}{i_d+i_r/N} \qquad (5)$$

where i_d and i_r are the disk and ring currents, respectively. N is the ring current collection efficiency, which is determined to be 0.37. The accelerated durability tests of the catalysts were performed in the O_2-saturated 0.1 M $HClO_4$ electrolyte at room temperature by applying potential cycling between 1.0 and 0.6 V vs. RHE at a sweep rate of 100 mV s^{-1} for 30,000 cycles.

Electrochemical measurements for fuel cell

Cathode catalyst inks were made by dispersing the $Pt_{1.5}Ni_{1-x}$/Ni-N-C catalysts in n-propanol, DI water, and 5% Nafion® suspension in alcohols at a 1:12:12:11 weight ratio, followed by high-speed homogenizer (20,000 rpm) for 1 hour and sonication treatment for 30 min to form catalyst slurry. The catalyst-coated-membrane (CCM) with an active geometric area of 12.25 cm^2 was applied to the carbon paper (Toray TGP-H-060) with an ultrasonic spray. The fabricated CCM was dried to completely evaporate the solvents. As for anode, Pt/C (20 wt % of Pt, JM Hispec3000) was used with loading of ~0.10 $mg_{Pt}\cdot cm^{-2}$. The prepared cathode and anode were pressed onto the two sides of a Nafion 211 membrane (DuPont) at 120 °C for 3 min under a pressure of 3 MPa by the hot press method to form the gas diffusion electrode (GDE). Two GDLs, two gaskets, and the prepared CCM were pressed to obtain the membrane electrode assembly (MEA). A control MEA of Pt/C catalyst was prepared in the similar way with a 0.10 $mg_{Pt}\cdot cm^{-2}$ Pt/C (20%) as the cathode. The fuel cell performance was measured with 850e Fuel Cell Test Station (Scribner Associates, Inc.) with absolute pressure of 1.5 bar for H_2 and air, using H_2 as the fuel and air as the oxidant under H_2/air conditions. The fuel cell performance was measured with 850e Fuel Cell Test Station (Scribner Associates, Inc.) with absolute pressure of 2.0 bar for H_2 and O_2, using H_2 as the fuel and O_2 as the oxidant under H_2/O_2 conditions. All the gases were humidified at 80 °C, 100% relative humidity, with the flow rate of 0.4 L min^{-1} for H_2 and 0.5 L min^{-1} for O_2. After the cell activates to a stable value, polarization curves were recorded with the increase in current density regularly.

Computation Methods

Our DFT calculations were performed via Vienna *ab initio* simulation package (VASP)[1].

The ion-electron interaction was described with the projector-augmented plane-wave (PAW) method[2]. Exchange-correlation energy were expressed by Perdew-Burke-Ernzerhof (PBE) functional with the generalized gradient approximation (GGA) [3]. The PtNi cluster was constructed with 41 Pt atoms and 6 Ni atoms. The PtNi cluster is randomly placed near the NiN_4 moiety decorated graphene layer to examine the preferred adsorption configuration. To avoid the interlayer interaction the vacuum layer set to be 20 Å. For geometry optimization, the cut-off energy was set to be 520 eV and the Brillouin zone was sampled with 1×1×1 k-points. The systems were relaxed until the energy and force reaching the convergence threshold of 10^{-4} eV and 0.03 eV/Å, respectively. We describe the van der Waals (vdW) interactions by utilizing the DFT-D3 method[4]. The electronic structures of the density of state (DOS) were calculated with 3×3×1 k-points.

Generally, the ORR involves four proton–electron transfer steps on the active sites, thus there are three different intermediate adsorbates: *OH, *O, and *OOH, the asterisk represents the adsorption site. The Gibbs free energy change ΔG of ORR on $Pt_{1.5}Ni_{1-x}$/Ni-N-C, $Pt_{1.5}Ni$/N-C, and Ni-N-C were evaluated by the formula:

$$\Delta G = \Delta E + \Delta ZPE + \Delta \int_{0}^{T} C_p dT - T\Delta S + \Delta G_U + \Delta G_{pH}$$

where ΔE is the adsorption energy of ORR intermediates and ΔZPE is their corresponding zero-point energy, ΔG_U is the free energy contribution induced by electrode potential U. ΔG_{pH} is the correction of the H^+ free energy by the concentration, which can be evaluated as $\Delta G_{pH} = 2.303 \times k_B T \times pH$ (or $0.06 \times pH$), here the value of pH was assumed to be zero. C_P is the constant-pressure heat capacity, the entropy and the integration terms are calculated based on the vibrational energies of ORR intermediates.

2. SUPPLEMENTARY FIGURES

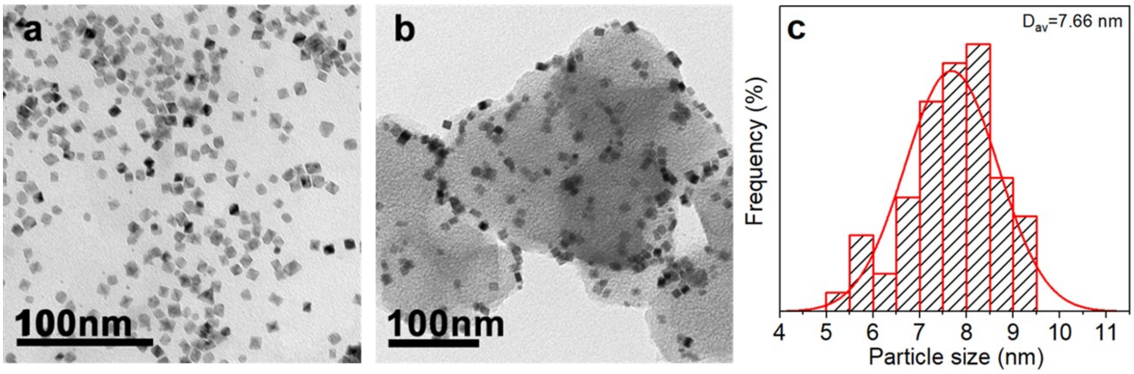

Supplementary Figure 1. TEM images of the (a)$Pt_{1.5}Ni$ NPs, (b)$Pt_{1.5}Ni$/N-C and (c) Statistics of nanoparticle size distributions of $Pt_{1.5}Ni$/N-C.

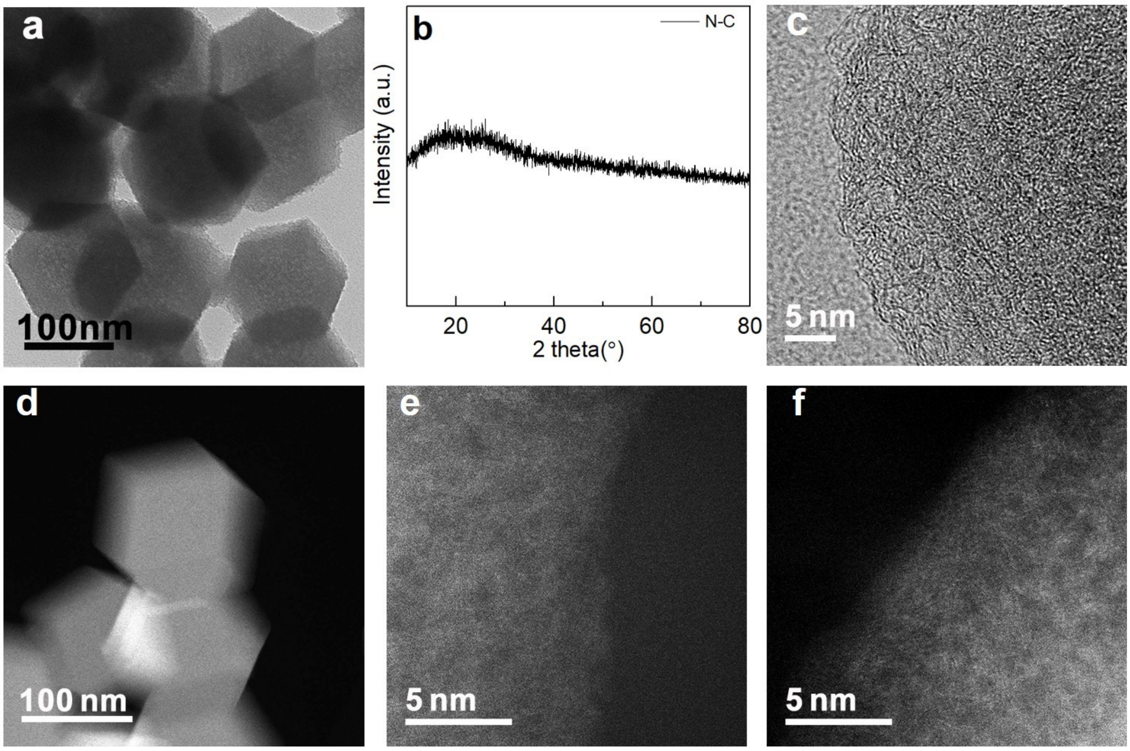

Supplementary Figure 2. (a) TEM image, (b) XRD pattern of Zif-8 derived N-C, (c) HRTEM image and (d-f) HAADF-STEM images of blank NC.

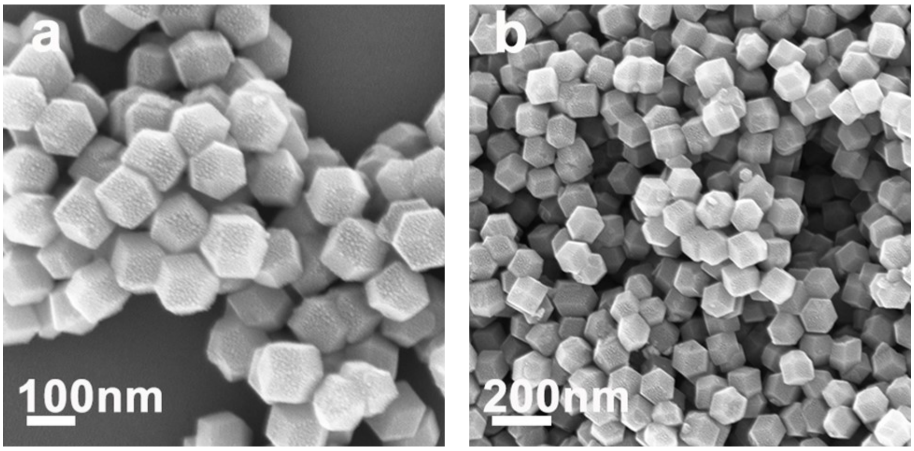

Supplementary Figure 3. SEM images of the $Pt_{1.5}Ni$/N-C.

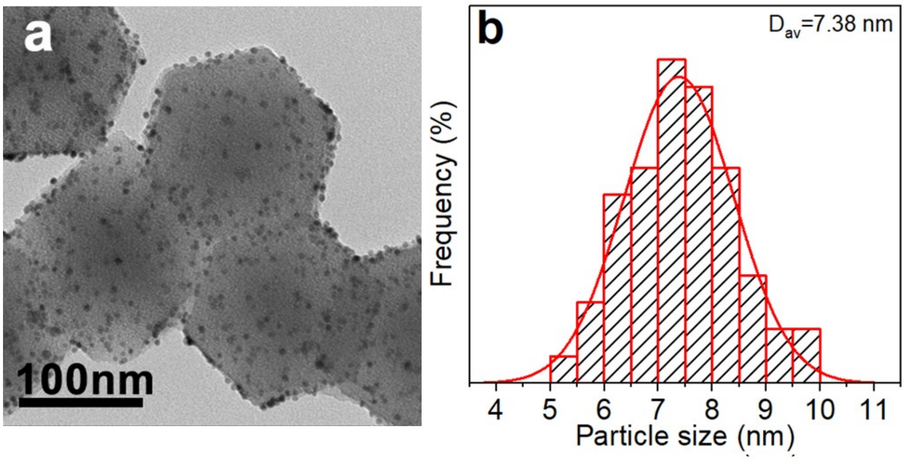

Supplementary Figure 4. (a) TEM image and (b)Statistics of nanoparticle size distributions of $Pt_{1.5}Ni_{1-x}$/Ni-N-C.

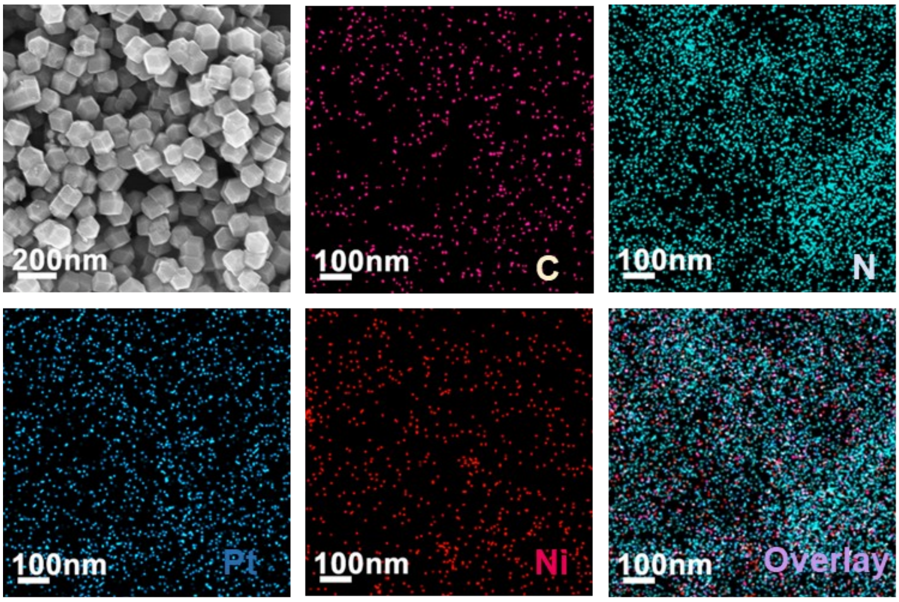

Supplementary Figure 5. SEM images and EDX-mapping images of $Pt_{1.5}Ni_{1-x}$/Ni-N-C sample. SEM images show that $Pt_{1.5}Ni_{1-x}$/Ni-N-C and $Pt_{1.5}Ni$/N-C shared similar intact rhombic dodecahedron morphology of ZIF-8 profile while the EDX-mapping indicates the distribution of different elemental contents.

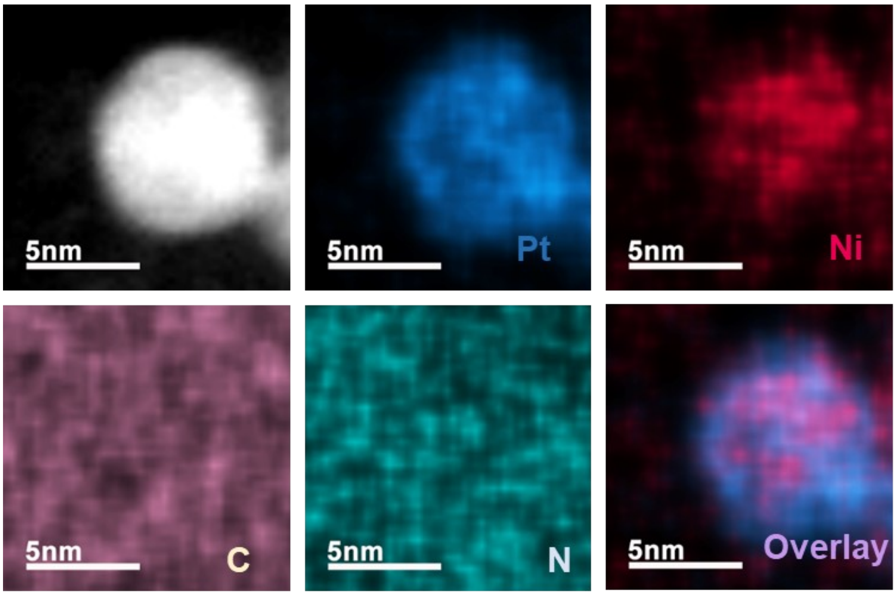

Supplementary Figure 6. STEM-EDX elemental mapping images of $Pt_{1.5}Ni_{1-x}$/Ni-N-C.

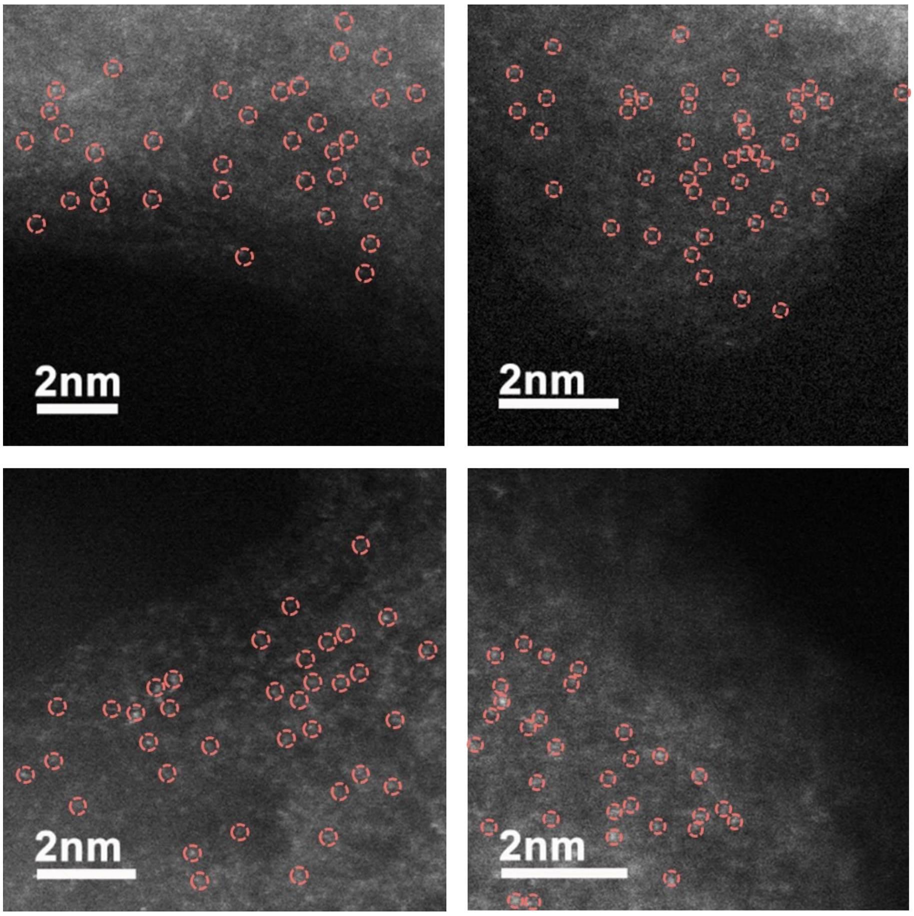

Supplementary Figure 7. AC HAADF-STEM images of $Pt_{1.5}Ni_{1-x}$/Ni-N-C.

AC HAADF-STEM images exhibit the existed of Ni SAs (circled in dark salmon) in different regions adjacent to particles on NC layer.

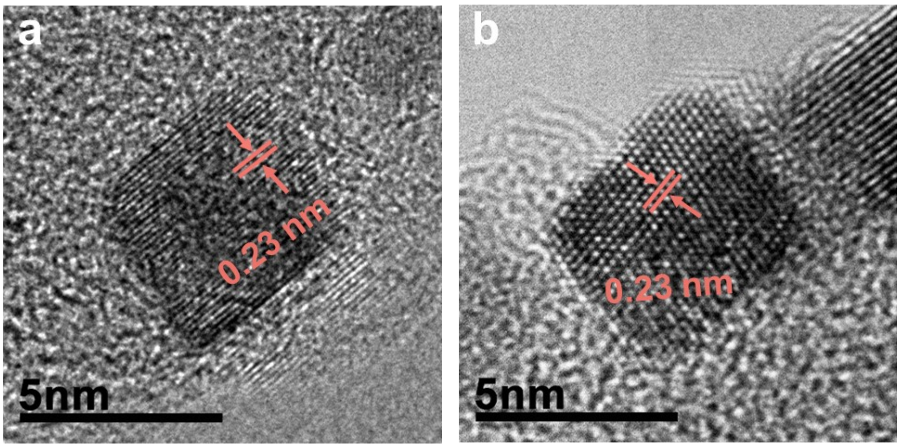

Supplementary Figure 8. HRTEM images of $Pt_{1.5}Ni$/N-C.

HRTEM images verify the $Pt_{1.5}Ni$ has an octahedral morphology and reveals a dominant (111) facets of $Pt_{1.5}Ni$ NPs.

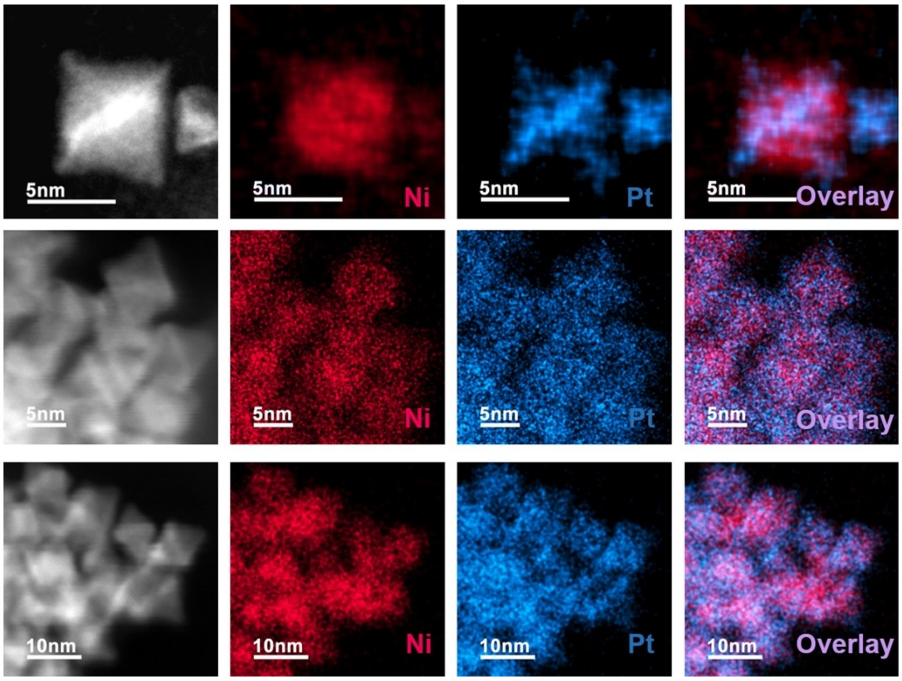

Supplementary Figure 9. STEM-EDX elemental mapping images of initial $Pt_{1.5}Ni$ NPs. STEM-EDX elemental mapping images reveal that the PtNi NPs show a uniform octahedral morphology at different scales, with Ni elements distributed on the surface and Pt elements mainly distributed on the edges.

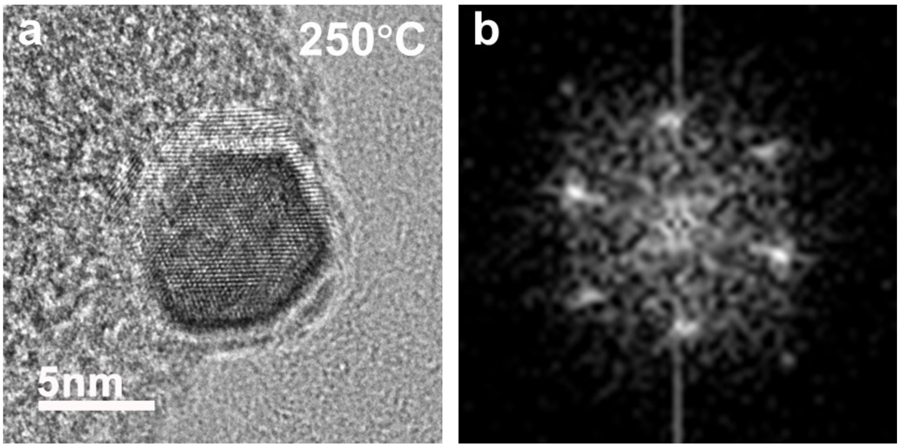

Supplementary Figure 10. (a) HRTEM image and (b)FFT of truncated octahedron $Pt_{1.5}Ni_{1-x}$/Ni-N-C treated at 250°C under NH_3 atmosphere.

HRTEM image shows a typical truncated octahedron morphology of the sample treated at 250°C and NH_3 atmosphere with mainly exposed (111) facets.

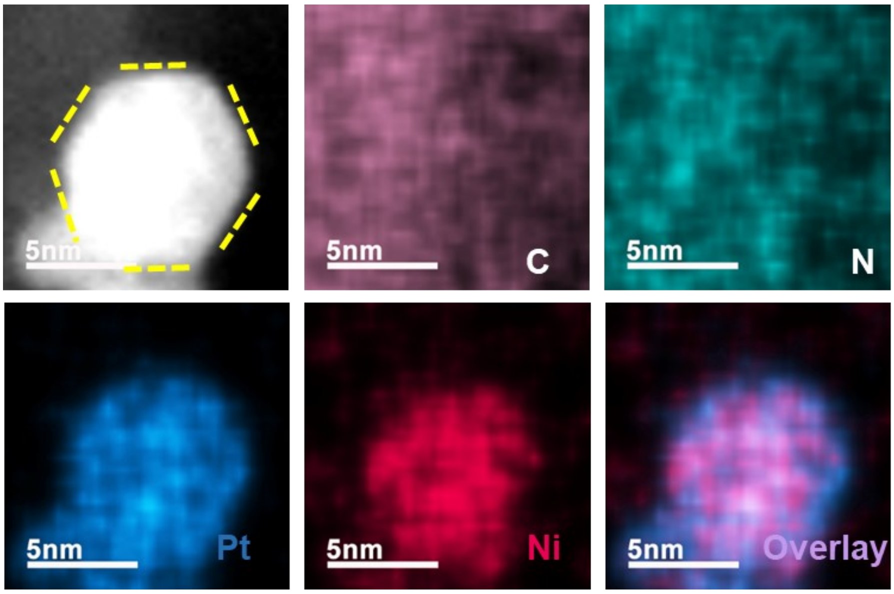

Supplementary Figure 11. STEM-EDX elemental mapping images of truncated octahedron $Pt_{1.5}Ni_{1-x}$/Ni-N-C treated at 250°C under NH_3 atmosphere.

EDS mappings reveal that the appearance of truncated octahedral PtNi NPs and Ni species were dispersed around the NPs, indicating that the Ni species were formed gradually during heating process in the presence of NH_3.

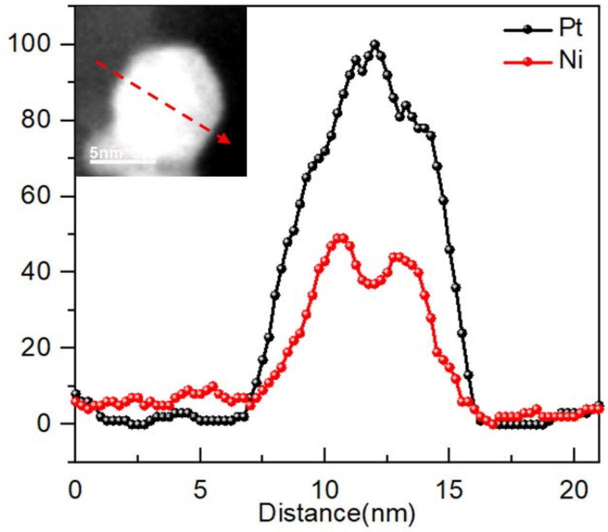

Supplementary Figure 12. Line scan of truncated octahedron $Pt_{1.5}Ni_{1-x}$/Ni-N-C treated at 250°C under NH_3 atmosphere.

Line scan plot of truncated octahedron $Pt_{1.5}Ni_{1-x}$/Ni-N-C demonstrates a surface layer with Pt-rich shell.

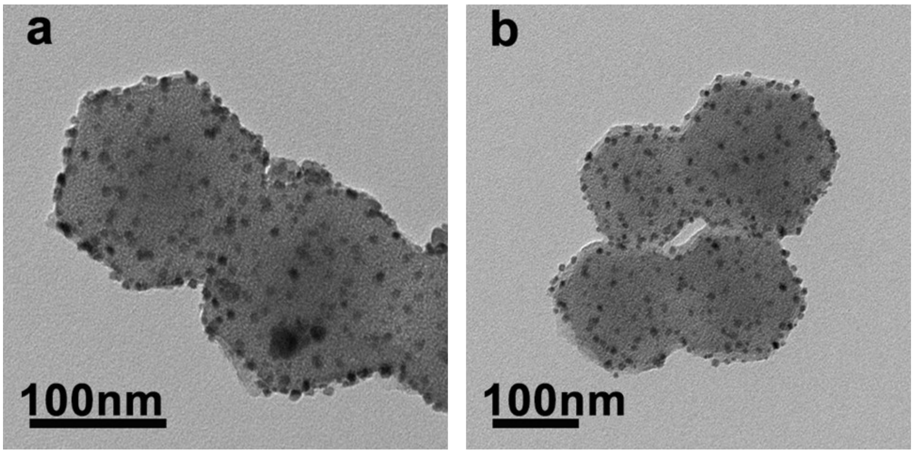

Supplementary Figure 13. TEM images of $Pt_{1.5}Ni_{1-x}$/Ni-N-C at 350°C under NH_3 atmosphere.

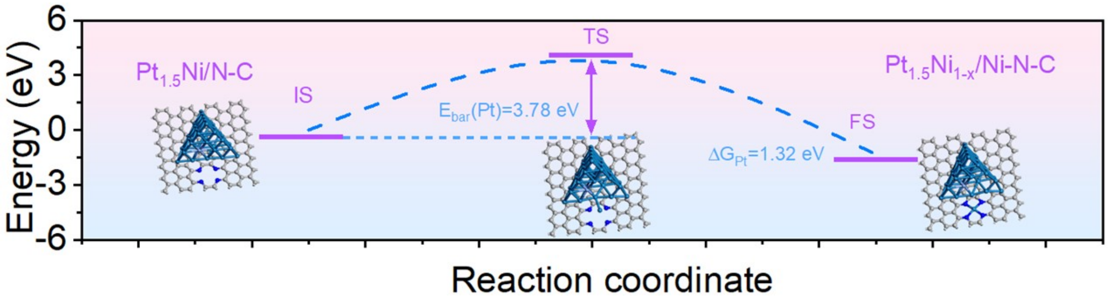

Supplementary Figure 14. Calculated energies along the stretching pathway of the Pt atom from the $Pt_{1.5}Ni$ cluster to Pt-N_4 sites by NH_3, and the corresponding initial and final configurations.

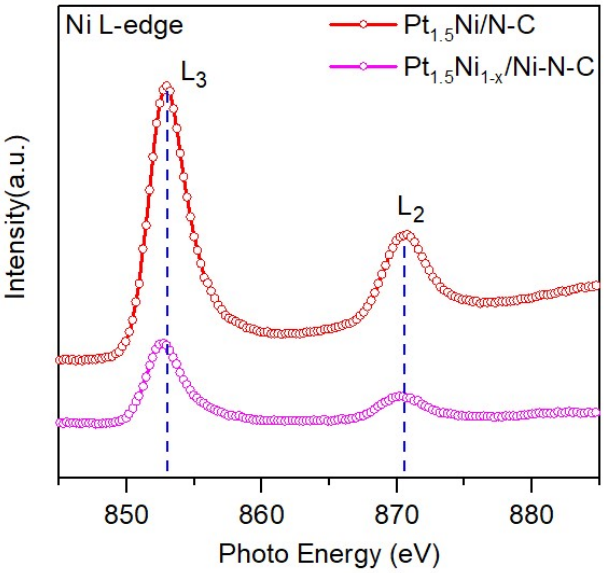

Supplementary Figure 15. Ni L-edge of $Pt_{1.5}Ni$/N-C and $Pt_{1.5}Ni_{1-x}$/Ni-N-C.

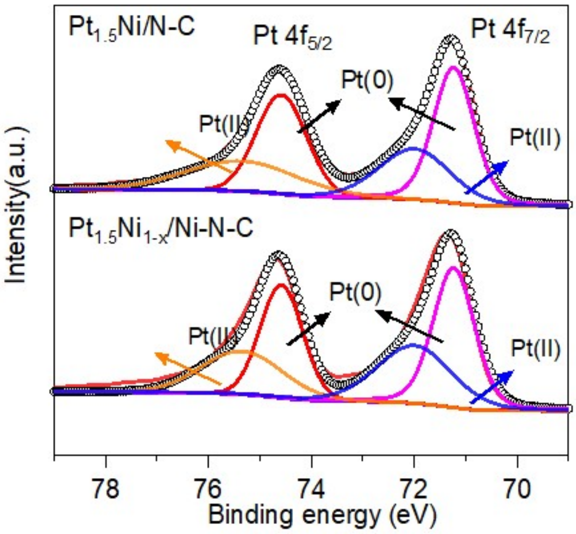

Supplementary Figure 16. XPS spectra of survey scan of Pt 4f XPS of the $Pt_{1.5}Ni$/N-C and $Pt_{1.5}Ni_{1-x}$/Ni-N-C.

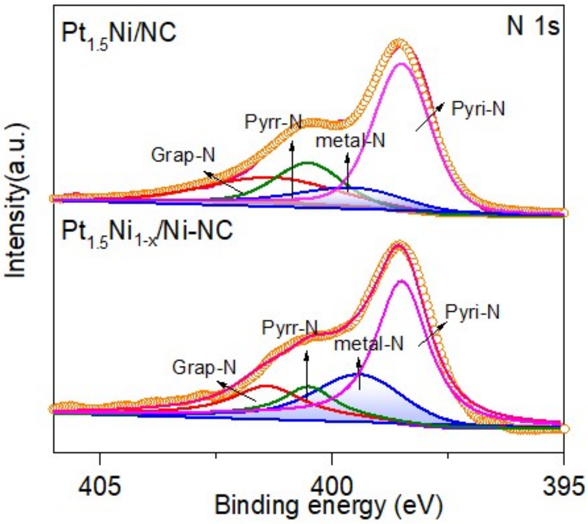

Supplementary Figure 17. XPS spectra of survey scan of N 1s XPS of $Pt_{1.5}Ni$/N-C and $Pt_{1.5}Ni_{1-x}$/Ni-N-C.

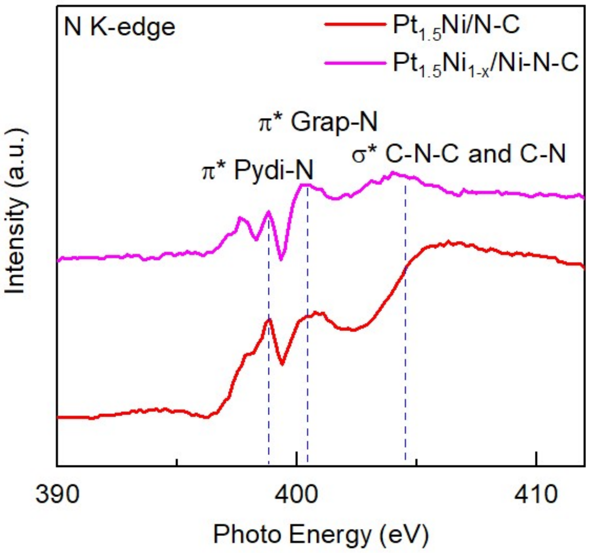

Supplementary Figure 18. N K-edge of $Pt_{1.5}Ni/N-C$ and $Pt_{1.5}Ni_{1-x}/Ni-N-C$.

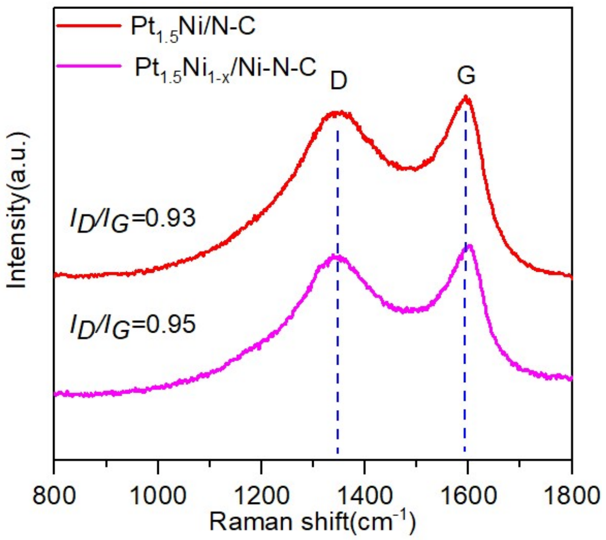

Supplementary Figure 19. Raman spectroscopy analysis of $Pt_{1.5}Ni/N-C$ and $Pt_{1.5}Ni_{1-x}/Ni-N-C$. The Raman spectroscopy analysis shows obvious carbon structure information in the disordered carbon (D,1341 cm^{-1}) and graphitic carbon (G,1597 cm^{-1}) bands, indicating the coexistence of graphite and defect-rich carbon components in this material. I_G is the area intensity in the G-band located at 1597 cm^{-1} corresponding to the zone center E_{2g} Raman activity mode of graphite and I_D is the area intensity in the D-band located at 1341 cm^{-1} corresponding to the vibrational density of the laminar sp^2 structure[5] 5. In this case, a high I_G/I_D ratio indicates a higher degree of graphitization. Here, Raman spectra show an increase in I_D/I_G values (0.93 vs 0.95) after treatment, indicating an increase in defect-rich carbon composition. This is because NH_3 is a very corrosive gas and has an etching effect on carbon materials[6-7]. During pyrolysis, NH_3 treatment can etch unstable Ni atoms to generate more disordered carbon, resulting in increased substrate porosity and reduced graphitization, which is one of the reasons for the good stability of the catalyst.

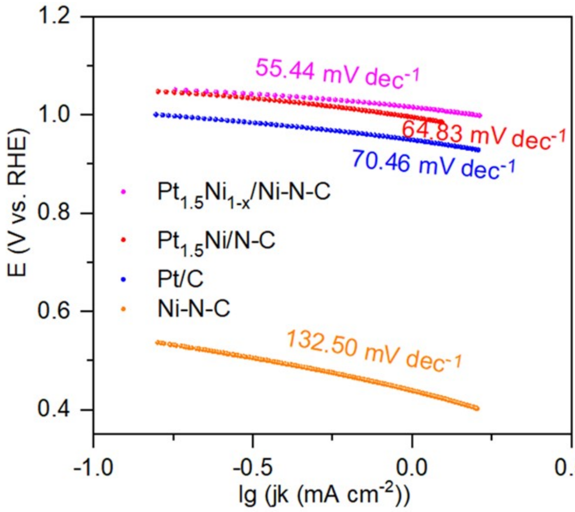

Supplementary Figure 20. The Tafel plots obtained from corresponding ORR polarization curves.

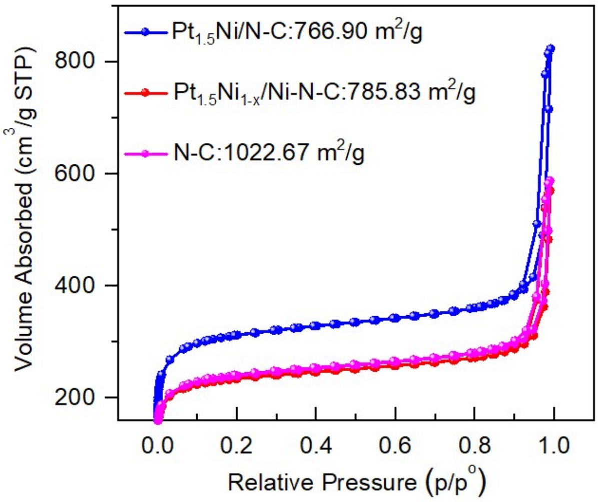

Supplementary Figure 21. The nitrogen absorption isotherm of $Pt_{1.5}Ni_{1-x}$/Ni-N-C, $Pt_{1.5}$Ni/N-C and N-C. The $Pt_{1.5}Ni_{1-x}$/Ni-N-C inherited a high specific surface area (785.83 m^2/g) of pyrolyzed ZIF-8 and was almost unchanged compared to $Pt_{1.5}$Ni/N-C (766.90 m^2/g).

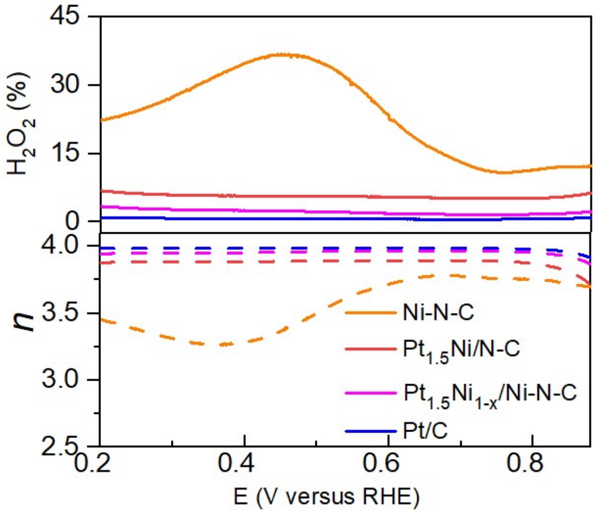

Supplementary Figure 22. Electron transfer number (n; bottom) and H_2O_2 yield (top) of Ni-N-C, $Pt_{1.5}Ni$/N-C, $Pt_{1.5}Ni_{1-x}$/Ni-N-C and commercial Pt/C.

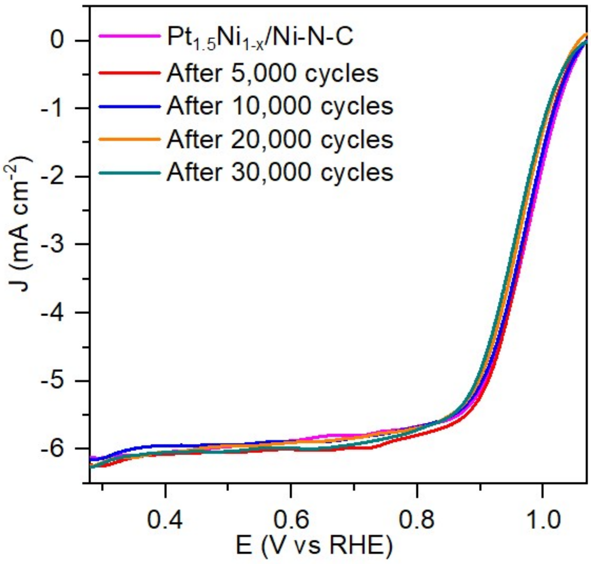

Supplementary Figure 23. ADT tests for $Pt_{1.5}Ni_{1-x}$/Ni-N-C after 5,000, 10,000, 15,000, 20,000 cycles.

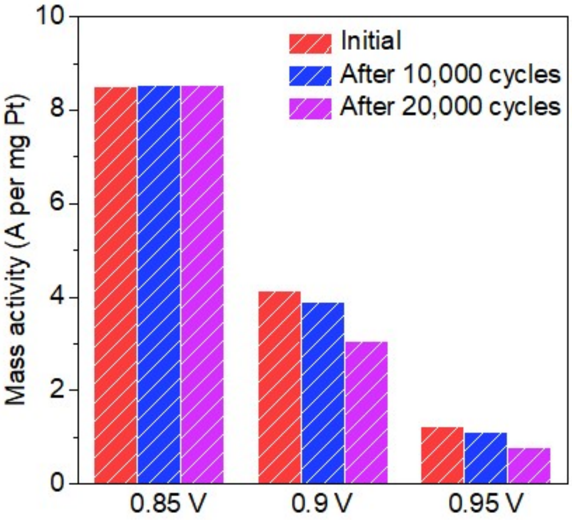

Supplementary Figure 24. Comparison of mass activities for $Pt_{1.5}Ni_{1-x}$/Ni-N-C at 0.9 V and 0.95V.

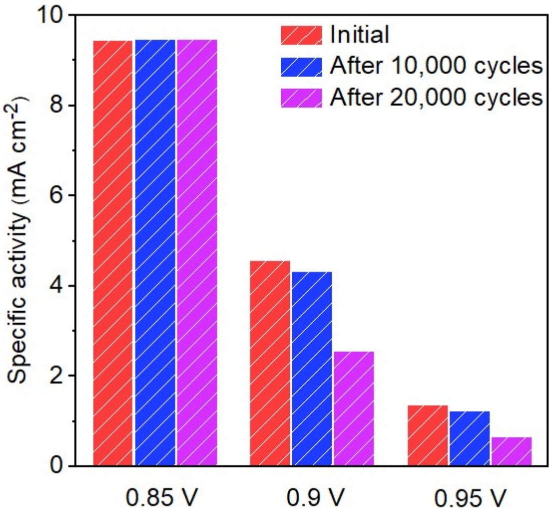

Supplementary Figure 25. Comparison of specific activities for $Pt_{1.5}Ni_{1-x}$/Ni-N-C at 0.9 V and 0.95V.

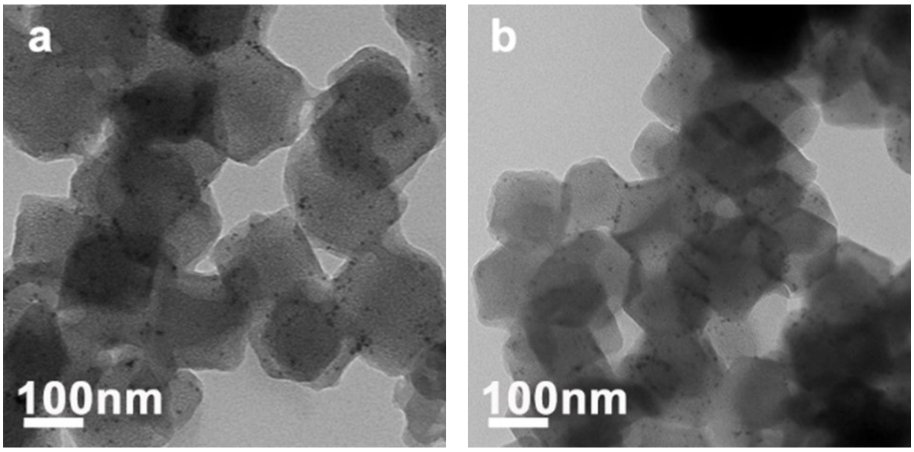

Supplementary Figure 26. (a-b) TEM images of the $Pt_{1.5}Ni_{1-x}$/Ni-N-C obtained after 30,000 ORR cycling test between 0.6 and 1.0 V.

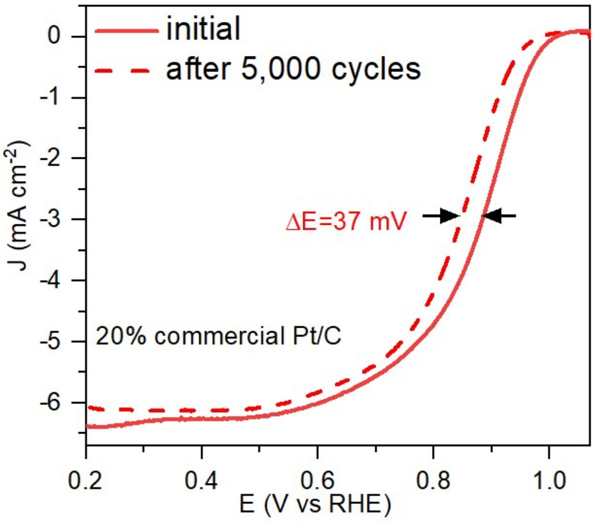

Supplementary Figure 27. ORR polarization curves of commercial Pt/C before (solid) and after (dot) 5000 cycles.

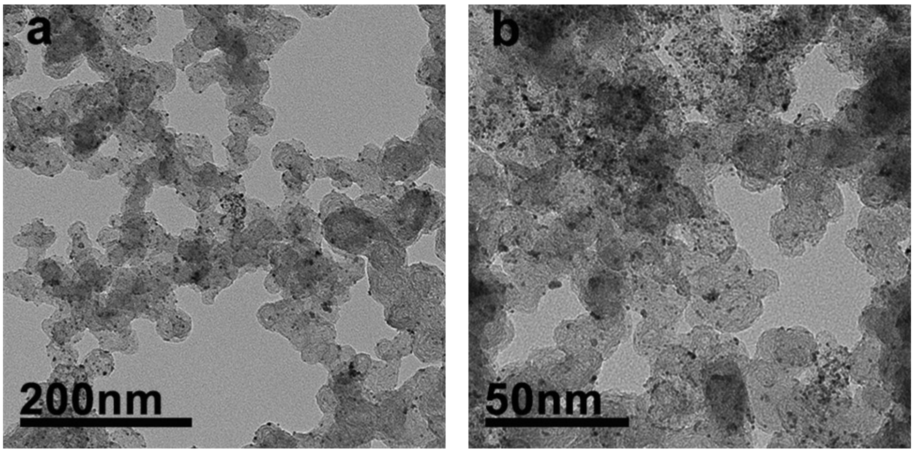

Supplementary Figure 28. TEM images of commercial Pt/C (A) before and (B) after ADT between 0.6 and 1.0V.

TEM images of commercial Pt/C show a significant sintering of Pt NPs after 5,000 cycles of testing, leading to a decrease in stability and activity.

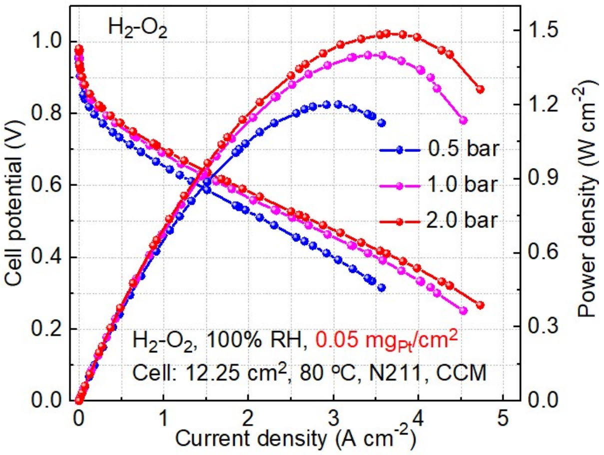

Supplementary Figure 29. H_2-O_2 fuel cell *i*-*V* polarization and power density plots recorded under 0.5bar, 1.0bar and 2.0bar O_2 pressure for $Pt_{1.5}Ni$/N-C.

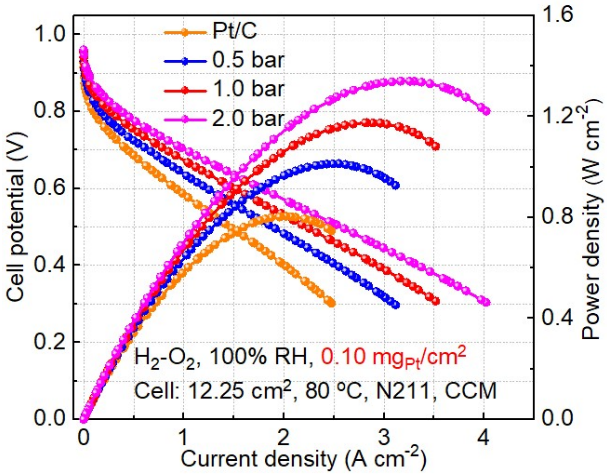

Supplementary Figure 30. H_2-O_2 fuel cell *i-V* polarization and power density plots recorded under no backpressure, 0.5bar, 1.0bar and 2.0bar O_2 pressure for commercial 20% Pt/C MEA.

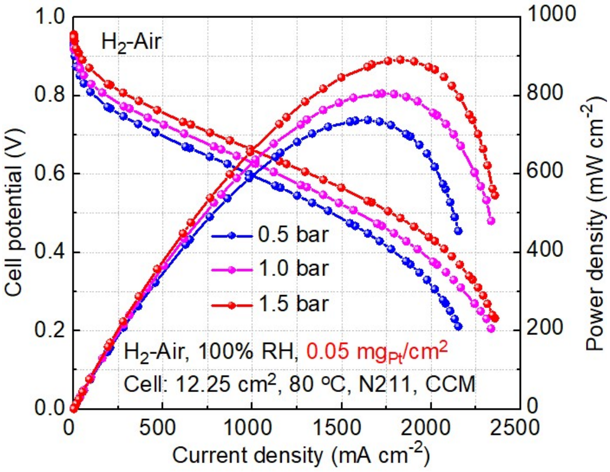

Supplementary Figure 31. H_2-Air fuel cell *i–V* polarization and power density plots recorded under different air pressure of $Pt_{1.5}Ni$/N-C.

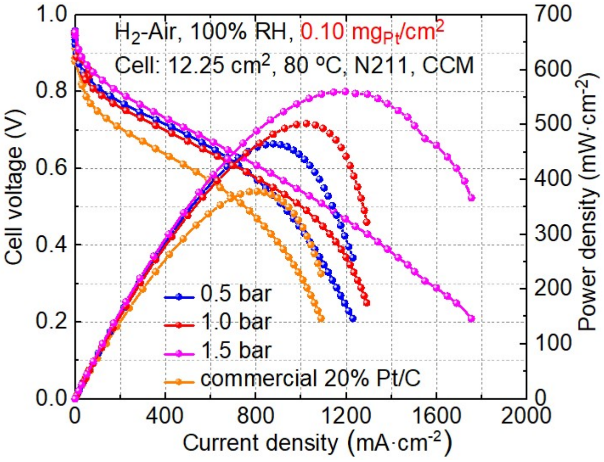

Supplementary Figure 32. H_2-Air fuel cell *i–V* polarization and power density plots recorded under different air pressure of commercial 20% Pt/C MEA.

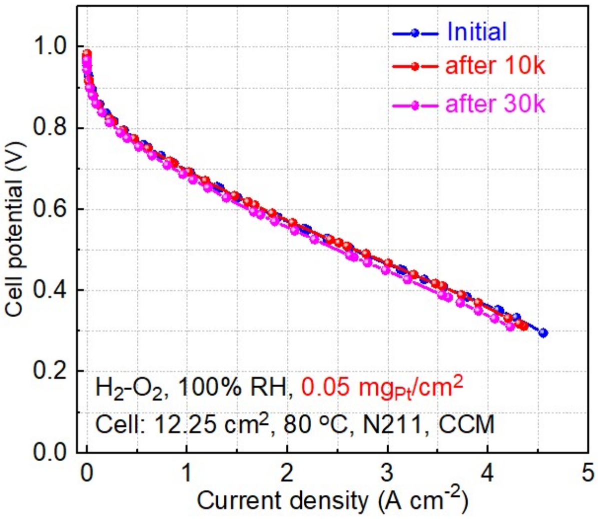

Supplementary Figure 33. ADT of $Pt_{1.5}Ni/N\text{-}C$ under H_2/O_2 at BOL, 10,000 and 30,000 cycles, respectively.

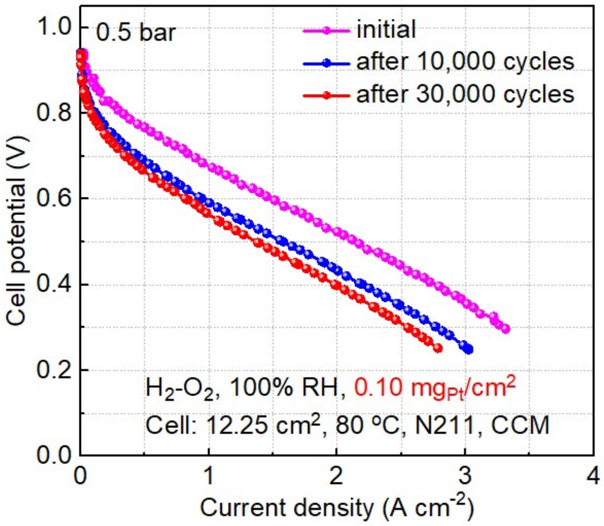

Supplementary Figure 34. ADT of commercial 20% Pt/C under H_2/O_2 at BOL, 10,000 and 30,000 cycles, respectively.

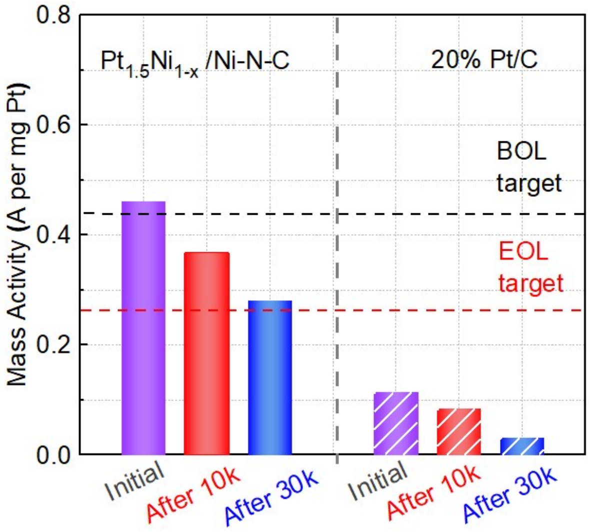

Supplementary Figure 35. Mass activity of $Pt_{1.5}Ni$/N-C and commercial 20% Pt/C at 0.9 V iR-free before and after ADT.

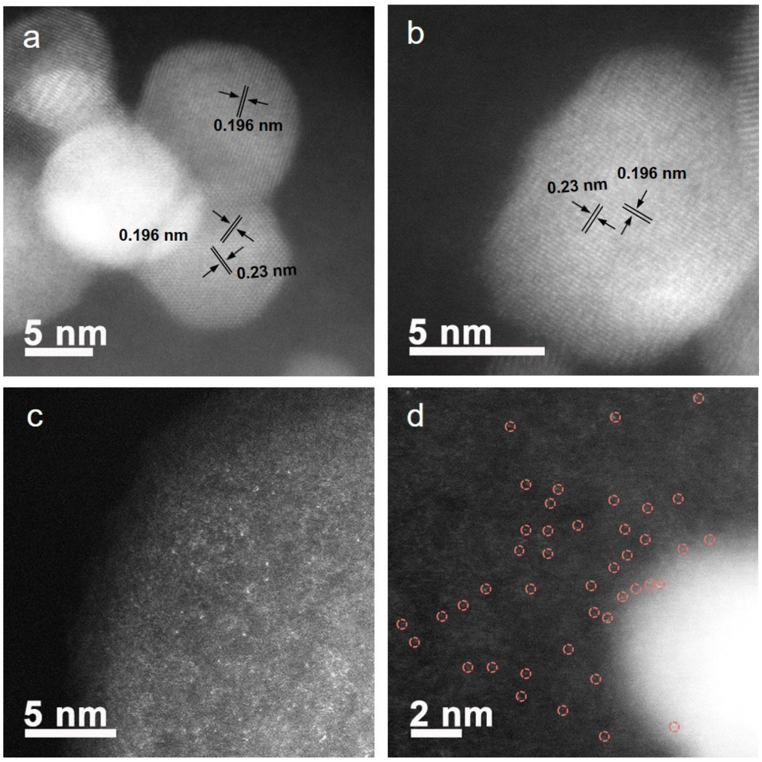

Supplementary Figure 36. a-b) HADDF-STEM images of Pt alloy NPs and c-d) Ni SAs in PtNi$_{1-x}$/Ni-N-C after ADT.

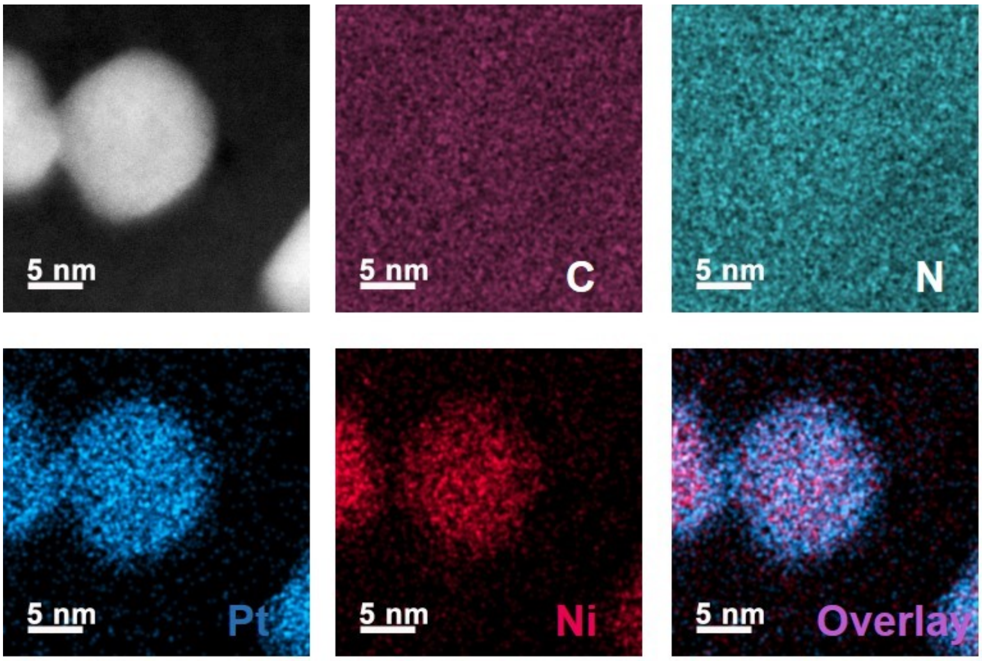

Supplementary Figure 37. HADDF-STEM and EDS mappings of PtNi$_{1-x}$/Ni-N-C after ADT.

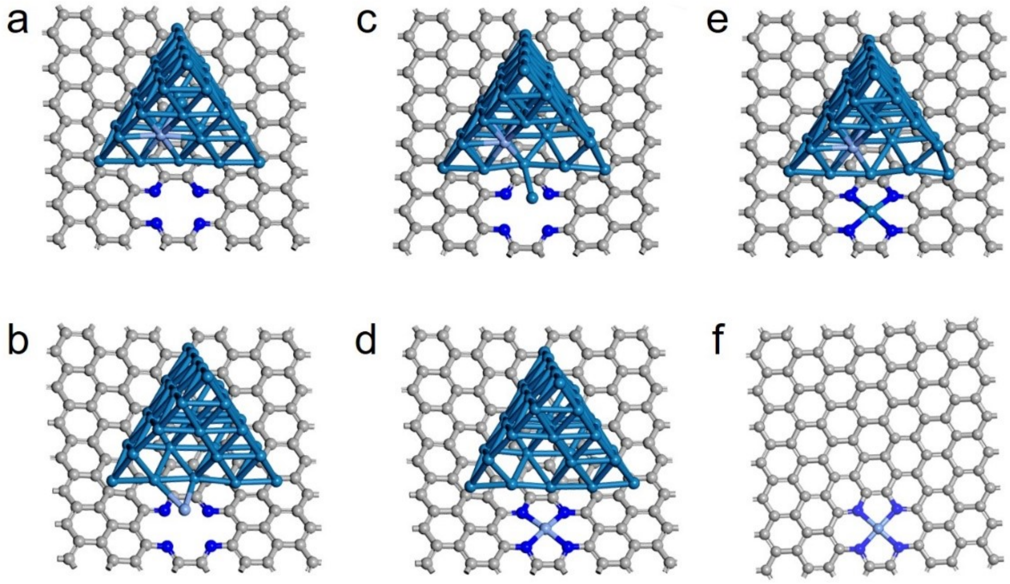

Supplementary Figure 38. The optimized geometry structures of (a) PtNi (111)/C, b) Ni atom migrate from PtNi (111)/C and (c) intermediate of Pt atom, (d) PtNi (111)/NiN$_4$, (e) PtNi (111)/PtN$_4$ and (f) NiN$_4$, respectively.

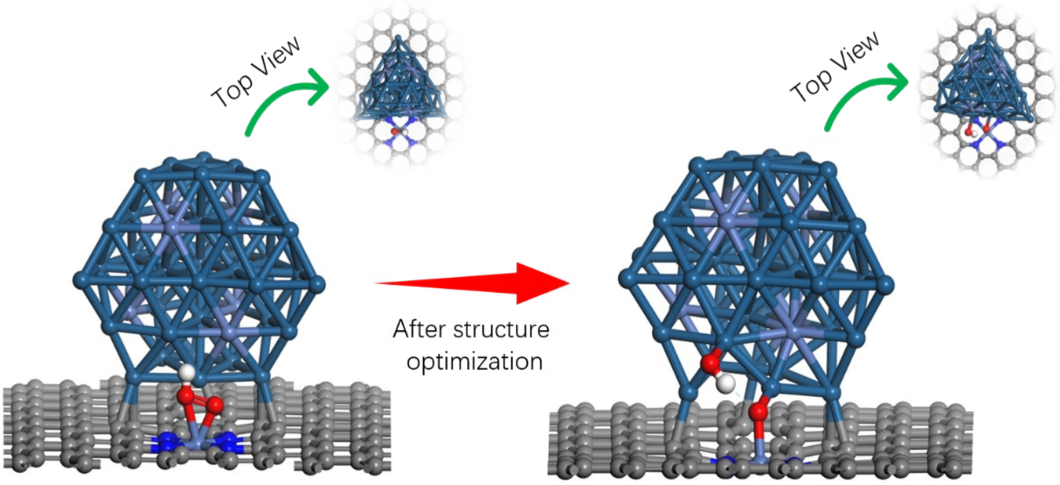

Supplementary Figure 39. Protonation of the adsorbed oxygen on the single Ni atom site neighboring the PtNi nanoparticles of the Pt$_{1.5}$Ni/Ni-N-C catalysts. The gray, blue, light blue, red, white, and dark green balls represent the C, N, Ni, O, H, and Pt atoms, respectively.

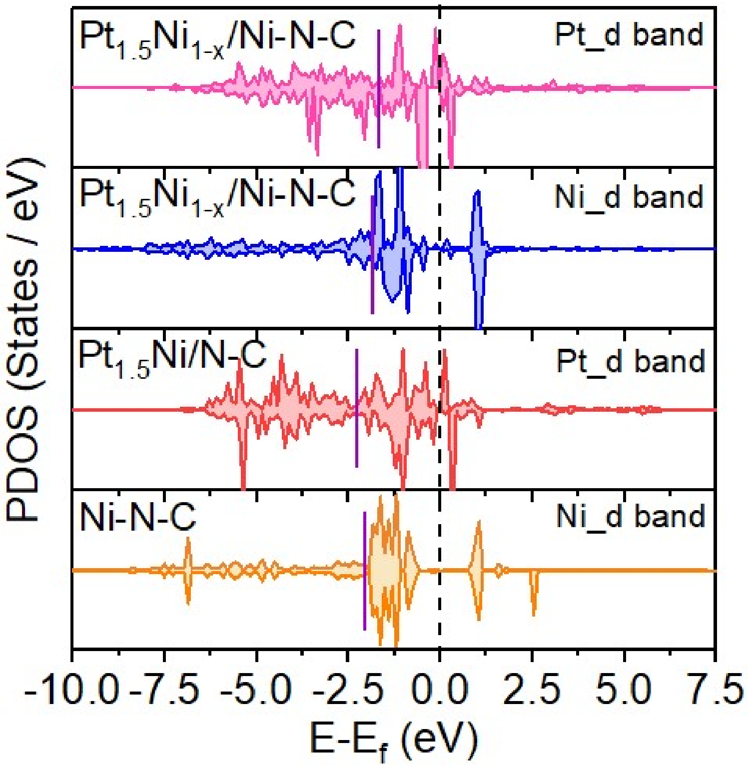

Supplementary Figure 40. The partial density of states and the corresponding d band centers of $Pt_{1.5}Ni_{1-x}$/Ni-N-C, $Pt_{1.5}$Ni/N-C and Ni-N-C. The Femi-level is marked with black dot line. The d band center is marked with purple line.

Supplementary Table 1. EXAFS fitting parameters at the Ni K-edge for various samples（S_0^2=0.76）

sample	shell	N^a	$R(Å)^b$	$\sigma^2(Å^2)^c$	ΔE_0(eV)^d	R factor
Ni foil	Ni-Ni	12	2.48	5.9	5.8	0.002
(1) Original $Pt_{1.5}Ni$/N-C	Pt-Ni	4.8	2.52	5.1	4.8	0.006
	Ni-Ni	8.0	2.48	6.6	5.6	
(2) treated at 150°C	Pt-Ni	4.1	2.54	7.5	4.2	0.004
	Ni-N	3.8	1.86	5.1	4.8	
	Ni-Ni	8.1	2.46	4.3	5.0	
(3) treated at 250°C	Pt-Ni	3.6	2.52	5.6	4.8	0.005
	Ni-N	4.1	1.86	7.1	5.2	
	Ni-Ni	7.9	2.46	7.4	5.3	
(1) $Pt_{1.5}Ni_{1-x}$/Ni-N-C	Pt-Ni	3.1	2.52	5.5	3.8	0.006
	Ni-N	4.1	1.87	5.8	4.0	
	Ni-Ni	7.8	2.45	6.9	4.5	

aN: coordination numbers; *bR*: bond distance; $^c\sigma^2$: Debye-Waller factors; $^d\Delta$E0: the inner potential correction. *R* factor: goodness of fit. S_0^2 was set to 0.831 for Pt, according to the experimental EXAFS fit of Pt foil by fixing CN as the known crystallographic value.

Supplementary Table 2. Comparisons of the mass activities compared to previously reported catalysts.

Catalyst	Catalyst loading (mgPtc m^{-2})	MA@0.9 V (A mgPt^{-1})	SA@0.9V (mA cm^{-2})	cycling stability	reference
$Pt_{1.5}Ni_{1-x}$/Ni-N-C	0.00800	4.10	8.30	20000 cycles	This work
Mo-Pt_3Ni/C	0.00408	6.98	10.3	8000 cycles MA~94.5% SA93.8%	*Science* **2015**, 348, 6240
PtPb Nanoplate /C	0.00638	4.3	7.8	50000 cycles MA~92.3%	*Science* **2016,** 354, 1410-1414
PtNi-BNCs/C	0.0068	3.52	5.16	50000 cycles MA~98.5%	*Science* **2019**, 366, 6467
Pd@Pt−Ni/C	0.0123	0.79	N.A.	6000 cycles 10%lost	*J. Am. Chem. Soc.* **2015**, 137, 2804
PtGa NWs	0.0128	1.89	3.28	30000 cycles MA~84.2%	*J. Am. Chem. Soc.* **2019,**

					141, 18083
37%FePt/ rGO	N.A.	1.96	4.1	20000 cycles	*J. Am. Chem. Soc.* **2020,** 142, 14190
Pd-Pt Tesseracts	0.0103	1.86	2.09	10000 cycles MA~92.6% SA~97.6%	*J. Am. Chem. Soc.* **2021**, 143, 496
Pt_3Co/FeN_4–C	0.13	1.34	3.98	30000 cycles	*Energy Environ. Sci.* **2020**, 13, 3032.
Ga-PtNi/C	0.025	1.24	2.53	30000 cycles MA~65.5%	*Nano Lett.* **2018**, 18, 2450.
MS-$Pt_{1.5}Ni$	0.00765	1.9	7.7	5000 cycles MA~90.2%	*ACS Catal.* **2020**, 10, 4205.

Supplementary Table 3. Comparisons of MEA-level ORR performances of our catalysts with those recently published catalysts.

Catalyst	Catalyst loading (mgPt cm^{-2})	Mass activity@0.9 V (A $mgPt^{-1}$) in H_2/O_2	Reference
$Pt_{1.5}Ni_{1-x}$/Ni-N-C	0.050	0.70	This Work
Pt-Fe-N-C	0.015	0.77	*Nature Catalysis* **2022**, 5, 503–512.
Pt-Ni UHT	0.066	0.49	*J. Am. Chem. Soc.* **2022***,* https://doi.org/10.1021/jacs.2c08361.
Pt-Co UHT	0.066	0.46	
Pt/N-KB 600 °C	0.110	0.20	*Nat. Mater.* **2020**, 19, 77.
Pt_A@FeSA-N-C	0.130	0.45	*Energy Environ. Sci.*, **2020**,13, 3032.
Pt_3Co/ FeN_4-C	0.130	0.72	*Energy Environ. Sci.*, **2020**,13, 3032.
$L1_0$-PtZn	0.100	0.52	*Adv. Energy Mater.* **2020**, 10, 2000179.
PtCo/C3	0.100	0.72	Matter, **2020**, 3,

PtNi/C3	0.100	0.66	1–17.
Int-PtNiN	0.120	0.49	ACS Catal. **2020**, 10, 10637
$L1_0$-CoPt/Pt	0.100	0.56	*Joule* **2019**, 3, 124.
W-doped $L1_0$-CoPt	0.110	0.57	*Angew. Chem. Int. Ed.* **2019**, 58, 15471.

References

1. Kresse, G.; Hafner, J., Ab initio molecular dynamics for liquid metals. *Phys Rev B Condens Matter* **1993,** *47* (1), 558-561.
2. Kresse, G.; Hafner, J., Ab initio molecular dynamics for liquid metals. *Phys Rev B Condens Matter* **1993,** *47* (1), 558-561.
3. Perdew, J. P.; Burke, K.; Ernzerhof, M. J. P. r. l., Generalized gradient approximation made simple. **1996,** *77* (18), 3865.
4. Grimme, S., Semiempirical GGA-type density functional constructed with a long-range dispersion correction. *J Comput Chem* **2006,** *27* (15), 1787-99.